Unusual first-order magnetic phase transition and large magnetocaloric effect in Nd$_2$In

Anis Biswas [1,*] Rajiv K. Chouhan [1] Alex Thayer,[1,2] Yaroslav Mudryk [1] Ihor Z. Hlova,[1]
Oleksandr Dolotko,[1,†] and Vitalij K. Pecharsky [1,2]

[1]*Ames National Laboratory, U.S. Department of Energy, Iowa State University, Ames, Iowa 50011, USA*
[2]*Department of Materials Science and Engineering, Iowa State University, Ames, Iowa 50011, USA*

A large magnetocaloric effect with its maximum near the boiling point of natural gas occurs in a rare-earth intermetallic compound Nd$_2$In. While behaviors of physical properties indicate that paramagnetic-ferromagnetic transformation supporting the large magnetocaloric effect is first order in nature, temperature-dependent crystallographic study reveals no changes in lattice symmetry and lack of discontinuities either in phase volume or lattice parameters. The borderline first-order nature of phase transformation in Nd$_2$In is markedly different from conventional first-order magnetic transitions occurring in other members of the family – isostructural Pr$_2$In and nonisostructural Eu$_2$In.

I. INTRODUCTION

Magnetocaloric refrigeration – a viable alternative to vapor-compression technologies – exploits reversible thermal, also known as magnetocaloric, effects (MCEs) that can be generated in magnetic solids by fluctuating magnetic fields with high efficiency. Advanced materials exhibiting large MCEs and systems that make use of the phenomenon attract strong interest in both basic (materials) and applied (material-system integration) research due to a potential the emerging solid-state magnetocaloric heat pumping technologies hold to mitigate adverse climate changes [1–5].

Paramagnetic materials, such as gadolinium sulfate [6], are common in adiabatic demagnetization refrigeration to achieve temperatures close to absolute zero, where heat capacities and lattice entropies of solids are negligible compared with the field-induced magnetic entropy changes. Heat pumping at higher temperatures, on the other hand, requires materials exhibiting phase transformations, where cooperative effects associated with global magnetic ordering or rearrangements thereof make it possible to induce functional MCEs even when lattice heat capacity approaches the Dulong-Petit limit, that is, in the presence of large lattice entropy. For example, proof of principle by Brown [7] and a number of laboratory-scale magnetocaloric cooling devices employ elemental gadolinium as an active material due to its large near-room temperature MCE that arises from a second-order ferromagnetic ordering phase transformation at 294 K [8].

Over the last few decades, substantial MCEs at ambient temperature and below have been reported in a number of rare-earth and transition-metal based compounds that undergo second-order magnetic phase transitions [9–16]. Yet, despite the abundance of reports characterizing MCE in solids, discovery of advanced materials that can be truly effective in applications ranging from near room temperature, including air conditioning and food storage, to cryogenic, such as liquefaction of gases, remains a major challenge. For heat-pumping applications below room temperature, compounds with large MCEs near the boiling point of natural gas are of particular interest considering continuous increase in the role of liquefied natural gas, consumption of which is predicted to double by 2040 [17]. Some of the rare-earth intermetallics where second-order magnetic phase transitions occur near the boiling point of natural gas include TbAl$_2$ [11], Dy$_{0.7}$Er$_{0.3}$Co$_2$ [12], and TbFeSi [13].

Compared with materials exhibiting second-order magnetic phase transitions, compounds that undergo first-order analogs may, and often do, exhibit much stronger thermal effects in practically achievable magnetic fields, known as the giant MCEs. In particular, the discovery of the latter in Gd$_5$Si$_2$Ge$_2$ led to a rapid expansion of research to solids with similar behaviors [18]. The transition that occurs in Gd$_5$Si$_2$Ge$_2$ is categorized as first-order magnetostructural transformation where the ferromagnetic ordering transition takes place conjointly with a rearrangement of chemical bonds and symmetry of the crystal lattice [19,20]. Similar transformations lead to giant MCEs in a number of other materials, which include MnTX (T is transition metal, X is $p-$block element) [21,22], MnAs$_{1-x}$P$_x$ [23], and Heusler alloys [24,25]. In addition to magnetostructural, first-order magnetoelastic transitions, during which crystallographic symmetry remains invariant and bonding is preserved, even though discontinuous changes in phase volume and/or lattice parameters are evident across the transition, are also known to result in a giant MCE [26]. Notable examples include La(Fe$_{13-x}$Si$_x$) and their hydrides [27], FeRh [28,29], and R_2In compounds, where $R =$ Eu and Pr [26,30,31].

─────────

*anis@ameslab.gov
†Present address: Karlsruhe Institute of Technology (KIT), Institute for Applied Materials-Energy Storage Systems (IAM-ESS), Hermann-von-Helmholtz-Platz 1, D-76344 Eggenstein-Leopoldshafen, Karlsruhe, Germany.

Since giant MCEs are associated with the first-order nature of the underlying phase transformations, functionality of materials exhibiting them may become impeded by thermomagnetic hysteresis, which results in energy losses during cycling [32]. In addition to hysteresis, brittle intermetallics may decrepitate as a result of cycling due to discontinuous phase-volume changes that occur across the transitions [19,21,22]. Mechanical instability of materials is a known barrier in many applications, including magnetocaloric heat pumping, where an active magnetic regenerator must remain intact for 100+ millions of field-up and field-down cycles. Conversely, thermomagnetic hysteresis and cycling failures are rare in materials exhibiting second-order phase transitions, even though both have been observed when crystallographic changes are continuous but substantial [33,34].

Thus, an ideal magnetic phase transition in a material with functional MCE would not be either a conventional first-order or a second-order phase transformation; rather, it would have certain characteristics of both of them. A nearly discontinuous change in magnetization ensuring large MCE, as observed during a first-order phase transition, is highly desired. At the same time, it should not be associated with measurable thermomagnetic hysteresis and large discontinuous crystallographic changes, like in a second-order material, to guarantee negligible energy losses [35,36], as well as the mechanical stability of a material [37]. One of the common approaches to achieve such transition is chemical modification of compounds with first-order phase transformations to minimize hysteresis and phase-volume change associated with the transitions and there are a few examples of materials where hysteresis was successfully addressed [27,28,38]. Most of those materials are transition-metal based and they exhibit first-order magnetoelastic transformations, but they are commonly quite brittle [27,38]. One example is hydrogenated La(Fe$_{13-x}$Si$_x$), where thermomagnetic hysteresis is manageable; however, at the same time the hydrides are fragile [37]. In this family of materials and in other transition-metal based compounds, magnetoelastic transformations are related to itinerant-electron metamagnetism [27].

In rare-earth based alloys and compounds the indirect Ruderman-Kittel-Kasuya-Yosida (RKKY)-type magnetic exchange interactions are dominant and the $4f-$element magnetic moments are localized, which makes them markedly different from the transition-metal based compounds, where magnetism is largely itinerant. Long-range magnetic order in lanthanide intermetallics depends on the $4f-5d$ hybridization and the exchange between $4f$ moments is mediated by itinerant s, p, and d electrons [39,40]. Itinerant electron metamagnetism, common for transition-metal based materials, is not expected in the lanthanide-based material systems without magnetic $3d$ metals, and as a consequence of that, first-order magnetoelastic transformations in $4f-$based compounds are uncommon. Yet, recent reports reveal their presence in R_2In compounds with $R =$ Eu and Pr, which are expected to be typical RKKY-type systems [26,30,31,41,42]. Here, symmetry-invariant crystallographic changes across the transition occur with minor discontinuities in lattice parameters and small, $\sim 0.1\%$, cell-volume changes that, in turn, lead to negligible hysteresis [26,30,31].

The discovery of anhysteretic first-order phase transitions in Eu$_2$In [26] and Pr$_2$In [30,31] was soon followed by further studies of similar rare-earth based systems in order to design new materials with large MCEs in the cryogenic temperature range and negligible hysteresis losses [43–45]. Recently, Liu *et al.* [44] and Cui *et al.* [45] reported similarly sharp and reversible magnetic phase transition in another R_2In compound with $R =$ Nd. The studies reveal large MCE in Nd$_2$In with its maximum close to the boiling point of natural gas. The nature of the phase transition in this compound is, however, not quite clear as some of the results of these two studies are contradictory. According to Liu *et al.* [44], Nd$_2$In undergoes a clearly first-order paramagnetic-ferromagnetic phase transition, while Cui *et al.* [45] rule out the occurrence of first-order phase change in Nd$_2$In. Thus, in this work, we revisit Nd$_2$In with experiments and first-principles theory to clarify the nature of the underlying phase transition that brings about a strong MCE.

II. EXPERIMENTAL METHODS

A. Sample preparation

A polycrystalline Nd$_2$In (3 g total mass) was prepared by arc melting stoichiometric amounts of pure metals in a Zr-gettered argon atmosphere. The Nd metal provided by the Materials Preparation Center of Ames National Laboratory [46] was 99.95 wt. % pure with respect to all other elements in the periodic table, whereas 99.995 wt. % pure indium was purchased from Alfa Aesar, USA. To ensure homogeneity, the alloy was remelted five times, flipping the button over after each melting. Weight loss after the melting was less than 0.5%. The arc-melted alloy was annealed at 973 K for 21 d in a quartz tube sealed under ~ 0.3 bar of high-purity helium. Then, the furnace was turned off and the alloy slowly cooled down to room temperature with the furnace. The prepared material was stored and handled in an argon-filled glovebox (MBraun Inc., USA) with oxygen and moisture levels below 1 ppm, anticipating its reactivity with ambient air from our prior experience in handling other R_2In compounds [26,30,31].

B. Powder x-ray diffraction

Both the room-temperature and the temperature-dependent powder x-ray diffraction (PXRD) study of Nd$_2$In were performed using a Rigaku TTRAX powder diffractometer equipped with a rotating anode Mo K$_\alpha$ source in the temperature range between 15 and 300 K; the details of the experimental setup are described elsewhere [47]. The Nd$_2$In was ground into powder in a glovebox and mixed with a petroleum jelly to prevent reaction of the powder with the atmosphere; once placed inside the PXRD equipment, the sample was kept in vacuum (10^{-4}–10^{-5} Torr). Rietveld refinements of the obtained PXRD data were carried out using FULLPROF [48].

C. Magnetization

A superconducting quantum interference device magnetometer, MPMS XL-7 (Quantum Design Inc., USA), was used to study magnetic properties of the material. The temperature

dependencies of DC magnetization, $M(T)$, were measured in the temperature range from 5 to 200 K in the presence of magnetic fields ranging between 100 Oe and 50 kOe. Prior to every set of measurements, the sample was cooled down to 5 K in the presence of a desired magnetic field and then M was measured as a function of T during the heating and cooling in that constant magnetic field. $M(T)$ data were recorded while approaching each temperature set point at ± 1 K/min, followed by a 5 s delay prior to measuring magnetization. The Curie temperature, T_C, was assigned as the temperature corresponding to the fastest change in $M(T)$, manifested as the minimum of $\partial M(T)/\partial T$. In order to assess magnetocaloric effect, we calculated isothermal magnetic-field induced entropy changes, ΔS, from the $M(T)$ data recorded in different magnetic fields using the Maxwell equation [49]. The magnetic ground state of the sample, saturation magnetization, and coercive magnetic field were examined via the magnetic-field dependence of magnetization, $M(H)$, measured at 5 K between -50 and 50 kOe.

D. Specific-heat study

In order to get additional insight into the nature of phase transitions and to fully evaluate MCE, heat capacity, $C_p(T)$, was measured in the temperature range between 2 and 100 K in several constant magnetic fields ranging from 0 to 50 kOe employing the relaxation method. A physical property measurement system (PPMS), manufactured by Quantum Design Inc., USA was employed for the specific-heat study. Both ΔS and adiabatic temperature change, ΔT_{ad}, were calculated from the $C_p(T)$ data to quantify MCE [50].

III. THEORETICAL METHODS

Spin-polarized density-functional theory (DFT) calculations [51] were performed within the local spin-density approximation (LSDA) plus U [52–55] approach using the full-potential linearized augmented plane-wave method as implemented in WIEN2k [56,57], where the Hubbard U correction is incorporated along with the generalized gradient approximation framework of Perdew *et al.* [58]. The Hubbard exchange parameter, $U_{eff} = 5$ eV, was chosen following previous studies [59,60] for proper treatment of the localized $4f$ electrons. The atomic radii for Nd and In are set as 2.5 bohr with force minimization of 1.0 mRy/a.u. The optimized value of plane-wave cutoff is obtained by setting $RK_{max} = 7.0$ and $G_{max} = 12$ with separation energies of -8.0 Ry between valence and core states as primary inputs into the WIEN2k-based LSDA + U calculations. The k−space integrations are done using the Brillouin-zone mesh of $19 \times 19 \times 13$, which is sufficient for the convergence of the total energies (10^{-6} Ry), charges, and magnetic moments. For comparison, we also repeated DFT calculations using similar method for Pr$_2$In (also see Ref. [31]) and Nd$_2$In with the Hubbard $U = 6$ eV. Densities of states of both Nd$_2$In and Pr$_2$In near the Fermi energy are practically independent of the selection of U between 5 and 6 eV.

IV. RESULTS AND DISCUSSION

A. Room-temperature crystallography

The PXRD pattern of Nd$_2$In recorded at room temperature [Fig. 1(a)] confirms the formation of a hexagonal Ni$_2$In−type structure (space group $P6_3/mmc$), same as that of Pr$_2$In [30,31], consistent with the previous studies [44,45,61]. About 5 wt. % of the Nd$_3$In phase was detected as an impurity, which is similar to the case of Pr$_2$In [30], where Pr$_3$In impurity is commonly found. As illustrated in Fig. 1(b), Nd atoms occupy two inequivalent sites: Nd1 in $2a$ with $x = y = z = 0$ and Nd2 in $2d$ with $x = 1/3$, $y = 2/3$, $z = 3/4$, whereas In atoms are located in $2c$ with $x = 1/3$, $y = 2/3$, $z = 1/4$. The room-temperature lattice parameters ($a = b = 5.5085 \pm 0.0007$ Å, $c = 6.8745 \pm 0.001$ Å) agree with the previously reported values for this compound [61].

B. Magnetic properties

The $M(T)$ data measured in a 1 kOe magnetic field [Fig. 2(a)] reveal a sharp, nearly discontinuous magnetic transition between the paramagnetic (PM) and ferromagnetic (FM) states at $T_C \cong 110$ K during both heating and cooling with very small thermomagnetic hysteresis (hysteresis width is less than 2 K). The observed sharpness of the transition is a typical characteristic of a first-order magnetic phase transition. It is worth recalling that a discontinuity in hyperfine field was observed in Nd$_2$In around ~ 110 K in an earlier study, also signifying the first-order nature of the magnetic ordering transition [40]. The transition remains sharp and reversible in a 20 kOe magnetic field [inset, Fig. 2(a)], but it becomes noticeably broader in higher magnetic fields [Fig. 2(b)]. With the application of magnetic field, T_C determined from the minima of $\partial M(T)/\partial T$ slowly shifts toward higher temperatures with $dT_C/dH \cong 0.14$ K/kOe [Fig. 2(b)].

In addition to the main transition at T_C and in agreement with the earlier study [62], $M(T)$ data show a second broad anomaly at $T_{SR} \sim 53$ K, where T_{SR} is spin-reorientation temperature [Figs. 2(a) and 2(b)]. We also note that the magnetic signature of the Nd$_3$In impurity, which orders ferromagnetically at 114 K [63], is not detectable in the $M(T)$ data of Fig. 2. Unlike T_C that is weakly dependent on magnetic field, there is hardly any change in T_{SR} as the magnetic field increases. The $M(T)$ behavior of the Nd$_2$In compound is qualitatively similar to that reported for Pr$_2$In [30,31], albeit both transitions in the latter occur at lower temperatures. Temperature dependence of inverse magnetic susceptibility (H/M) is linear above T_C, following the Curie-Weiss law with an effective magnetic moment $p_{eff} \cong 5.18\,\mu_B$/f.u. ($3.67\,\mu_B$/Nd as there are two independent Nd sites in Nd$_2$In), in good agreement with the calculated theoretical $p_{eff} = g\sqrt{J(J+1)} = 3.62\,\mu_B$/Nd for noninteracting Nd^{3+}. The Weiss temperature is $\theta_p \cong 99$ K, which is slightly lower than T_C.

Figure 2(c) shows isothermal magnetization measured at $T = 5$ K, confirming the ferromagnetic ground state with saturation magnetic moment of $2.47\,\mu_B$/Nd, which is smaller than the expected $gJ = 3.28\,\mu_B$/Nd. The presence of crystalline electric field (CEF) in Nd$_2$In [40] can be responsible for the experimentally observed lower than theoretical value of the saturation magnetization. Smaller value of experimental
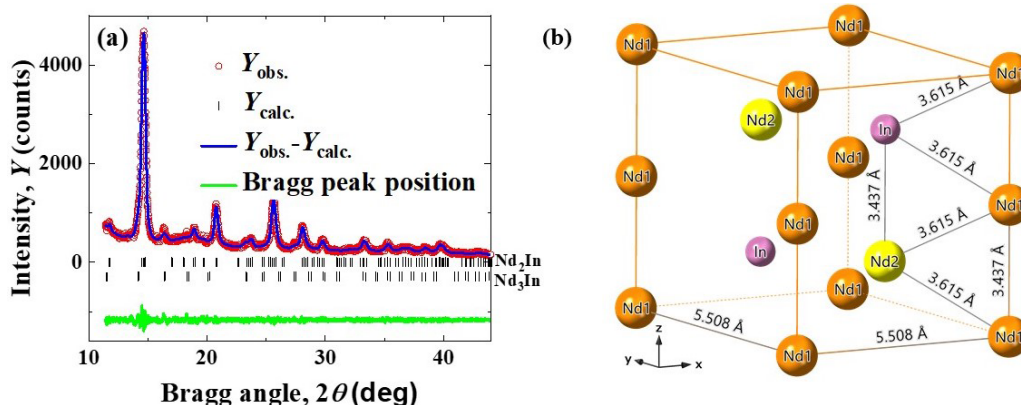
FIG. 1. (a) Rietveld-refined room-temperature PXRD pattern of Nd_2In measured using Mo K_{α} radiation. (b) Perspective view of the hexagonal Ni_2In-type crystal structure (space group $P6_3/mmc$) showing selected nearest-neighbor distances at room temperature.

saturation magnetic moment is also observed in Pr_2In [30,31]. Another important feature here is weak but measurable coercive field ($H_C \approx 700$ Oe), indicating weak magnetocrystalline anisotropy, which is in contrast to the $M(H)$ behavior of Pr_2In where much larger H_C of ~ 5 kOe at 5 K was observed [30,31].

C. Magnetocaloric effect

The sharp magnetic transition at T_C signifies strong MCE in Nd_2In. Quantified as ΔS calculated from $M(T)$ data measured in different applied magnetic fields, the effect is, indeed, large, with $\Delta S_{max} = -13$ J/Kg K for $\Delta H = 20$ kOe at $T_C = 110$ K, increasing to $\Delta S_{max} = -18$ J/Kg K for $\Delta H = 50$ kOe [Fig. 3(a)]. While ΔS_{max} of Nd_2In is lower compared to $\Delta S_{max} = -28.2$ J/Kg K observed in Eu_2In [26] at 55 K for the same $\Delta H = 20$ kOe, it is comparable to, or larger than, MCEs reported for the majority of known rare-earth based intermetallic materials, including other R_2In compounds between 40 and 150 K [Fig. 3(b)] [11–14,26,30,64–68]. Further, $|\Delta S_{max}|$ of this Nd_2In sample is considerably larger than that reported in both previous studies [44,45] due to a sharper transition and a larger jump of magnetization at T_C because of higher purity of the Nd metal used in this study when compared to the typical 99.9 wt. % purity (usually quoted with

respect to other rare earths) by commercial vendors. It is a high value reported at temperature close to the boiling point of natural gas [Fig. 3(b)] [11–13,44]. Since the magnetic transition at T_C is associated with nearly negligible hysteresis, the energy losses are expected to be negligible. Magnetocaloric effect associated with the spin reorientation at ~ 53 K is much weaker, as expected.

From the observed asymmetric broadening of $-\Delta S(T)$ around T_C at higher ΔH [inset, Fig. 3(a)], a typical feature of first-order phase transition [18], one can assume that magnetic transition at T_C for Nd_2In is of first-order type. The thermodynamic nature of a magnetic phase transition at T_C has been further probed through the analysis of magnetic-field dependence of ΔS [69]. In general, magnetic-field dependence of ΔS can be described by the power law [69,70]: $\Delta S \propto H^n$, where the exponent, n, can be calculated as

$$n(H,T) = \frac{d \ln|\Delta S|}{d \ln(H)} \tag{1}$$

The H and T dependencies of n for Nd_2In illustrated in Fig. 3(c) show maxima with $n > 2$ near T_C, which are characteristic features of the first-order magnetic phase transition [69]. Thus, apart from the observed sharpness of the transition and asymmetric broadening of $-\Delta S(T)$, the field dependence of ΔS indicates that the magnetic transition at T_C
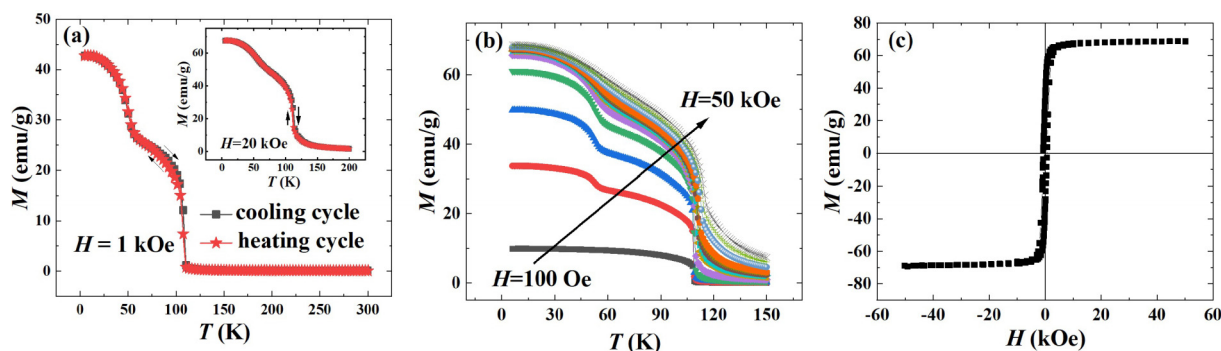
FIG. 2. (a) Temperature dependence of magnetization of Nd_2In measured during heating and cooling in 1 kOe magnetic field showing nearly negligible hysteresis at T_C; (Inset) $M(T)$ of the same sample recorded in 20 kOe magnetic field during heating and cooling. (b) $M(T)$ data of Nd_2In measured in different magnetic fields ranging from 100 Oe to 50 kOe during heating. (c) Magnetic-field dependence of magnetization, $M(H)$, recorded at 5 K.
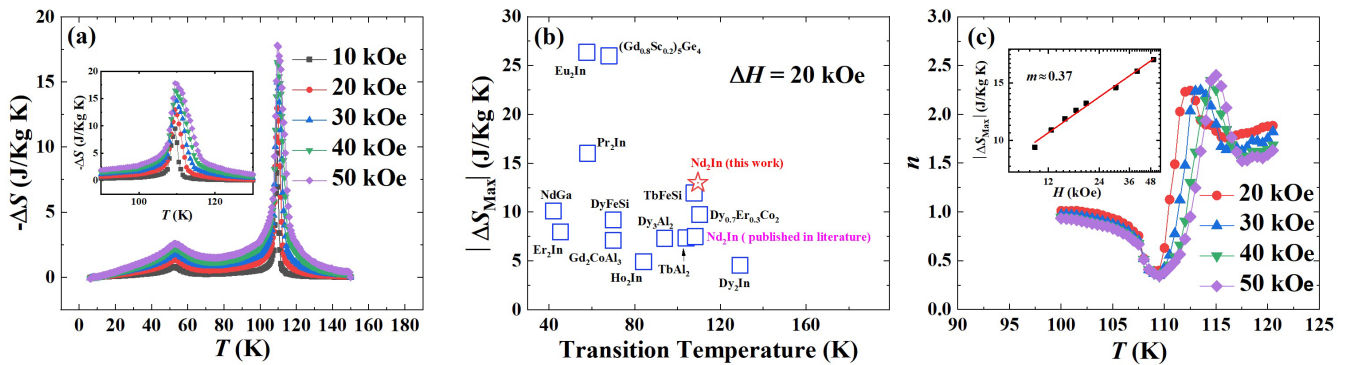
FIG. 3. (a) Temperature dependence of $-\Delta S$ of Nd_2In for $\Delta H = 10, 20, 30, 40,$ and 50 kOe. (Inset) Expanded view of the main peak around T_C. (b) Comparison of $|\Delta S_{max}|$ of Nd_2In for $\Delta H = 20$ kOe with those reported in related R_2In and other rare-earth compounds (R = rare earth) known to exhibit strong magnetocaloric effects between 40 and 150 K [11–14,26,30,64]. (c) Temperature dependence of exponent n defined in Eq. (1) for different magnetic fields; (Inset) Linear double-logarithmic plot of the maximum entropy change (ΔS_{max}) vs H with slope $m \approx 0.37$.

for Nd_2In is first order, as was observed in both Pr_2In and Eu_2In [26,30,31]. This conclusion is in agreement with the work of Liu *et al.*, who also characterized the phase transition in this compound as first order [44]. Yet, our analysis contradicts the $n(H, T)$ behavior reported by Cui *et al.* [45].

We further analyze the field dependence of the maximum magnetic-field induced entropy change, $|\Delta S_{max}|$. As reported, $|\Delta S_{max}|$ is expected to follow a power-law dependence on H with the exponent $m < 2/5$ for first-order and $m > 2/5$ for second-order phase transformations [71]. The inset of Fig. 3(c) illustrates a linear double-logarithmic plot confirming the power-law dependence with the slope $m \approx 0.37$. This value is slightly lower than 2/5, characterizing the transition at T_C as first order. At the same time, close proximity of m to 2/5 also implies that the transition is likely borderline between first- and second-order.

D. Heat capacity

The thermodynamic nature of a phase transition can also be directly probed by $C_p(T)$ measurements. Here, a first-order transformation is manifested as theoretically infinite heat capacity, in reality very high, sharp, and narrow, nearly symmetrical peak at the transition temperature and a clear, nearly isothermal step in $S(T)$. Both anomalies reflect the presence of latent heat during the transition [72] that is, by definition, absent in case of second-order phase transformations. As illustrated in Fig. 4(a), with the temperature resolution typical for a standard 2τ analysis of raw heat-capacity data measured in PPMS [26], a strong and sharp, but highly asymmetric, nearly $\lambda-$shaped peak is observed in $C_p(T)$ near T_C in $H = 0$. The rise of the entropy is rapid, yet it occurs without a clear isothermal step around T_C [inset, Fig. 4(a)]. Indicative of a second-order phase transition, this behavior contradicts the conclusion about the first-order nature of ferromagnetic ordering inferred from the analysis of magnetic behaviors in low fields and MCE, as well as hyperfine-field data published earlier [40]. A second broad peak is visible in $C_p(T)$ at ~ 53 K [Fig. 4(a)] in agreement with the $M(T)$ anomaly observed around same temperature reported to be a spin-reorientation transition in a prior study [62]. With the

application of magnetic field, the $\lambda-$shaped peak in $C_p(T)$ near T_C gradually broadens but it also clearly shifts to higher temperatures [inset, Fig. 4(b)], confirming rising T_C; the latter is not expected for second-order ferromagnetic ordering transformations.

The maximum ΔS calculated from the heat-capacity data is -14 J/Kg K for $\Delta H = 50$ kOe that, within experimental errors typical for the two techniques [50], matches -18 J/Kg K calculated for the same field change from magnetization data. The behavior of the adiabatic temperature change calculated from the heat-capacity data illustrated in Fig. 4(b) reflects a second-order nature of the phase transition at $\sim T_{SR}$ (a caret-like peak rising and broadening symmetrically with the increasing field). At T_C, on the other hand, a highly asymmetric broadening of the $\Delta T_{ad}(T)$ peak is consistent with similar asymmetric broadening of $\Delta S(T)$ [inset, Fig. 3(a)] commonly associated with first-order phase transitions. Heat capacity, total entropy, and adiabatic temperature change data, therefore, indicate that the transition at T_C is intermediate between first- and second-order in nature.

E. Low-temperature crystallography

Generally, if a transition between PM and FM phases is first order, a discontinuous change in lattice volume is expected. When a transition is second order, no such discontinuities should occur, albeit a few examples of materials with strong but continuous changes of lattice parameters are known, e.g., GdNi [34]. Since our magnetization and specific-heat data do not provide unambiguous evidence regarding the thermodynamic nature of the magnetic ordering transition at T_C in Nd_2In, we further investigated the temperature dependence of its crystal structure in the temperature range 15–295 K. As an example, Fig. 5(a) shows a PXRD pattern of Nd_2In recorded at 15 K, which only reflects shifts of the Bragg peaks due to thermal expansion, but otherwise is identical to that recorded at room temperature [Fig. 1(a)].

Thus, the Ni_2In-type crystal structure is retained below both T_C and T_{SR}, similar to the case of Pr_2In [29]. Figures 5(b), 5(c), and 5(d) illustrate temperature dependences of cell volume and lattice parameters a and c, respectively. In agreement
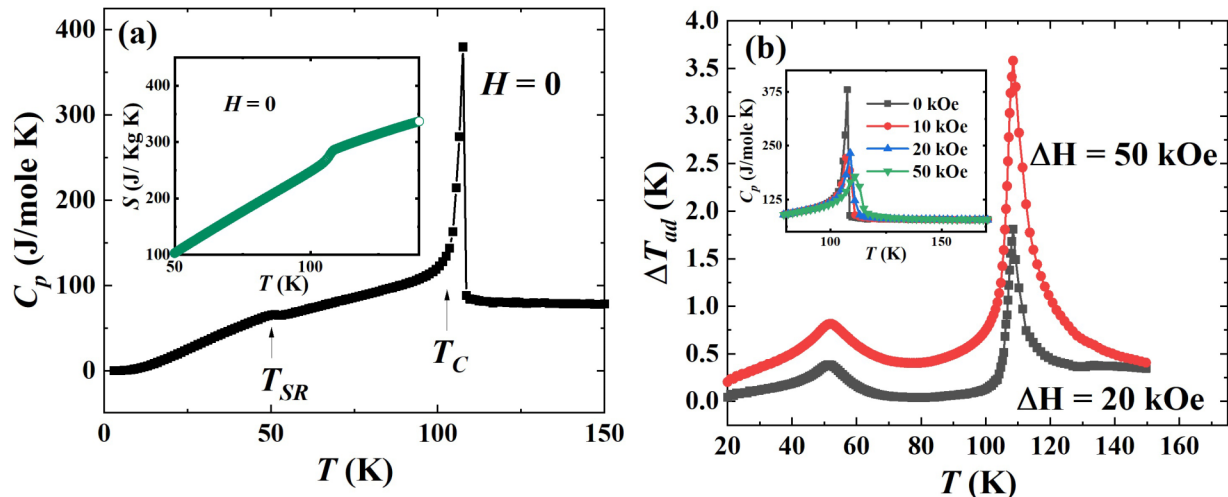
FIG. 4. (a) Temperature dependence of heat capacity of Nd_2In measured in $H = 0$. The ferromagnetic transition temperature, T_C, and the temperature corresponding to the spin-reorientation anomaly, T_{SR}, are indicated by arrows. (Inset) Temperature dependence of the total entropy calculated from $C_p(T)$. (b) Temperature dependence of ΔT_{ad} of Nd_2In for $\Delta H = 20$ and 50 kOe. (Inset) $C_p(T)$ data of Nd_2In recorded in 0, 10, 20, and 50 kOe magnetic fields. Only the temperature range near the T_C is shown in the inset for clarity.

with the results of Cui *et al.* [45], the PXRD study does not reveal any crystal symmetry change in the studied temperature range (15–300 K), and Nd_2In does not exhibit discontinuities in either phase volume or lattice parameters at T_C in contrast to Pr_2In and Eu_2In [26,31]. Thermal expansion is anisotropic, and below T_C it is enhanced for V and a but becomes arrested for c. The changing slopes of the temperature dependencies of phase volume and lattice parameters below T_C indicate that while weak magnetoelastic coupling is present, it is not strong enough to result in a discontinuous change of V. Taken together with all other experimental results described above, one can conclude that a magnetoelastic transition in Nd_2In at T_C is borderline between first order and second order, showing some features characteristic of the former, while other features are characteristic of the latter, making a large MCE observed here favorable for applications.

F. Theory

Even though both Nd_2In and Pr_2In exhibit similar magnetic behaviors and large magnetocaloric effects, the underlying ferromagnetic ordering transitions are apparently different in nature. To further clarify the observed differences, we performed DFT calculations for both Pr_2In and Nd_2In using unit-cell dimensions of the latter determined at 15 K and those determined at 6 K [31] for the former as inputs into DFT. These are the lowest temperatures where experimental crystallographic data for the two compounds adopting the same Ni_2In-type crystal structure are available and, noting that all of the atoms occupy sites without coordinate degrees of freedom, the corresponding unit cells are assumed to represent the ground-state structures, i.e., at $T \rightarrow 0$ K.

Spin-polarized calculations imposing collinear ferromagnetism of Nd_2In yield magnetic moments of 3.73 and 3.08 μ_B, respectively, for Nd1 and Nd2; both are larger than the average 2.47 μ_B/Nd moment estimated from experiment at 5 K. This discrepancy is attributed to the presence of CEFs [40] that are

not accounted for in DFT. Figure 6 compares the density of states (DOS) of Nd_2In with that of Pr_2In, revealing a markedly different behavior near the Fermi energy (E_F). For clarity, Figs. 6(a) and 6(b) show total DOS, highlighting $4f-$electron contributions, while Figs. 6(a') and 6(b') show the partial indium $5p$ and lanthanide $5d$ DOS near the Fermi energy.

In Pr_2In, $4f$ states of Pr1 (the numbering of atoms is identical to that used for Nd_2In in Sec IV A) lead to a large total majority DOS at E_F [peak marked 7 in Fig. 6(b)], whereas the same peak is located just below E_F in Nd_2In [labeled 1 in Fig. 6(a)]. Furthermore, the majority $4f$ DOS of Pr1 is split into two groups around E_F [marked 5, 6, and 7 in Fig. 6(b)]. Conversely, similar splitting of $4f$ states corresponding to Nd2 is evident above E_F, labeled 2, 3, and 4 in Fig. 6(a). Most importantly, $4f$ states in Pr_2In just below (peak 6) and just above E_F (peak 7) and their hybridization with Pr $5d$ and In $5p$ states results in peaks 6' and 7' in the majority DOS, Fig. 6(b'). Hence, $5d$ electrons play a dominant role in mediating magnetic interactions between the local $4f$ moments in Pr_2In. Similar hybridization of Nd $4f$ with Nd $5d$ and In $5p$ states [peak labeled 2' in Fig. 6(a')] occurs slightly above E_F, weakening contributions of $5d$ and $5d-5p$ hybridized states near E_F in Nd_2In. For the minority DOS, there are no $4f$ states near E_F and features like those described above are absent in both compounds.

The stronger d states contributions near E_F in Pr_2In when compared to Nd_2In are experimentally observed in recent electronic transport studies as well [45]. While both materials exhibit negative magnetoresistance related to changes in $5d$ electron DOS at E_F with application of external magnetic field, a sharp peak in the temperature dependence of negative magnetoresistance at T_C is larger in Pr_2In [45]. The lanthanide $5d$ and indium $5p$ hybridization with strong d character near E_F is also evident in the majority-spin DOS of Eu_2In, and it is believed to play a vital role in the occurrence of first-order magnetoelastic transition in that
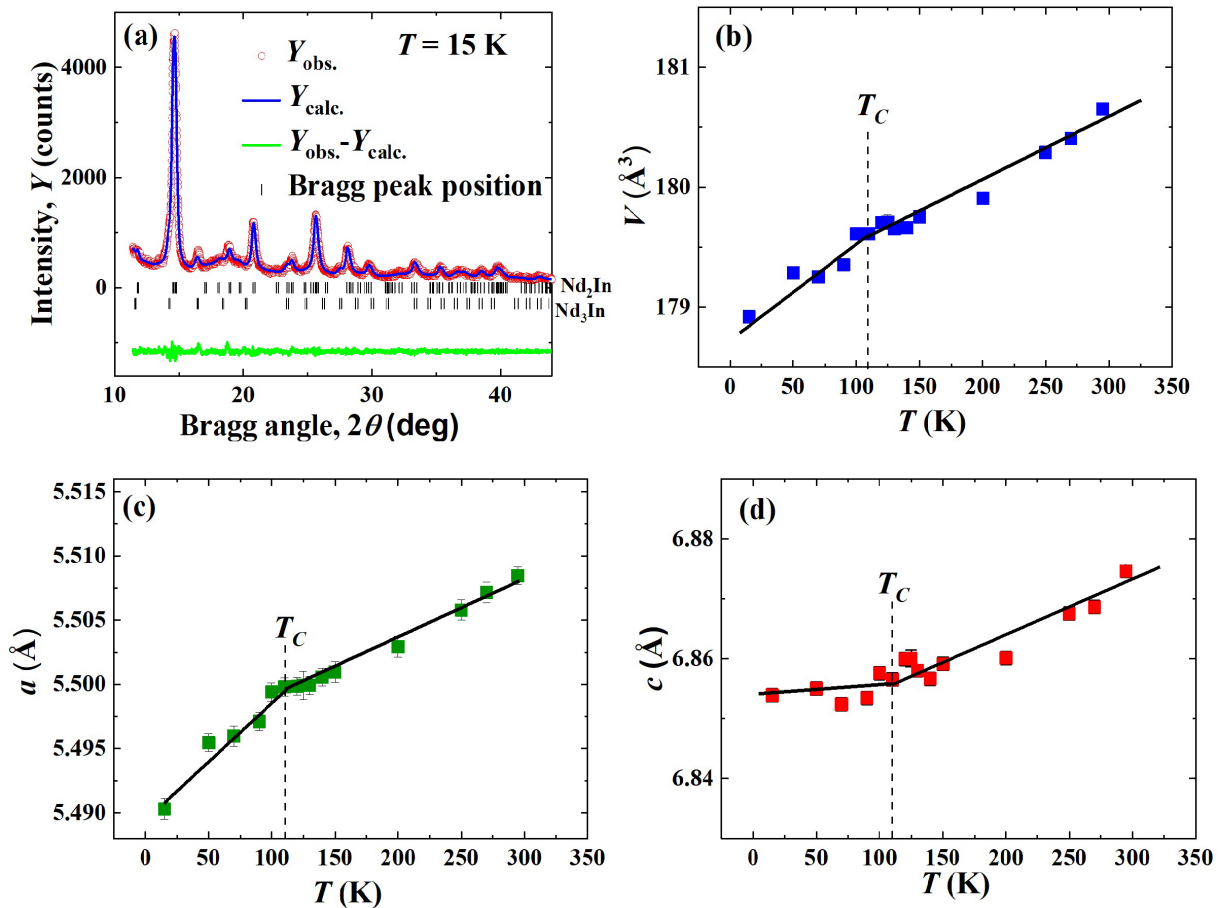
FIG. 5. (a) Powder x-ray diffraction pattern of Nd_2In measured at 15 K. (b), (c), and (d), respectively, illustrate the temperature dependencies of unit-cell volume, V, lattice parameters $a(= b)$, and c. The solid lines in (b), (c), (d) are used to guide the eye. No discontinuous change either in V or in any lattice parameter is observed around T_C.
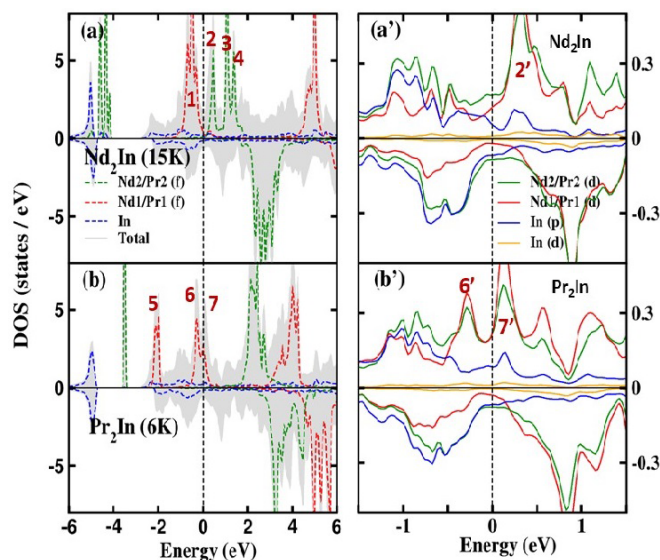
FIG. 6. DOS of (a) Nd_2In and (b) Pr_2In [31] calculated using lattice parameters of Nd_2In experimentally determined at $T = 15$ K and of Pr_2In experimentally determined at $T = 6$ K [29]. Panels (a') and (b') show site-specific partial DOS for indium d and p states, and neodymium and praseodymium d states near E_F. See text for the meaning of numerals 1−7 and 2', 6', and 7'.

compound, which nominally lacks $5d$ electrons because Eu is divalent [73]. Furthermore, $5d$ and $5p$ states are split near E_F in Eu_2In [73], making it similar to what is seen in Pr_2In [peaks 6' and 7' in Fig. 6(b')]. Hence, in analogy with Eu_2In [73], one can assume that Pr $5d$−In $5p$ hybridization and its strong d character near E_F is instrumental in the occurrence of first-order magnetoelastic transition in Pr_2In. In this context, we also recall that lanthanide $5d$−indium $5p$ hybridization occurs much below E_F in Gd_2In that, while adopting the same hexagonal structure as Pr_2In and Nd_2In, has antiferromagnetic ground state, but where the high-temperature transition between paramagnetic and ferromagnetic states is clearly second order [73].

Both similarities and differences between Pr_2In and Nd_2In are further reflected in the Fermi surface topologies. As illustrated in Figs. 7(d) and 7(h), three bands in the majority-spin channel (shown as vertical bars) cross E_F in both compounds. These bands include contributions from the rare-earth $4f$, rare-earth $5d$, and indium $5p$ states at the Fermi energy. The major difference is that the bands crossing E_F in Pr_2In are more localized around E_F making the corresponding Fermi surfaces topologically different from those in Nd_2In.

For clarity, panels (a)–(c) and (e)–(g) in Fig. 7 show contributions from the individual bands, marked in panels (d) and (h), to the Fermi surface in the first Brillouin zone. Panels on
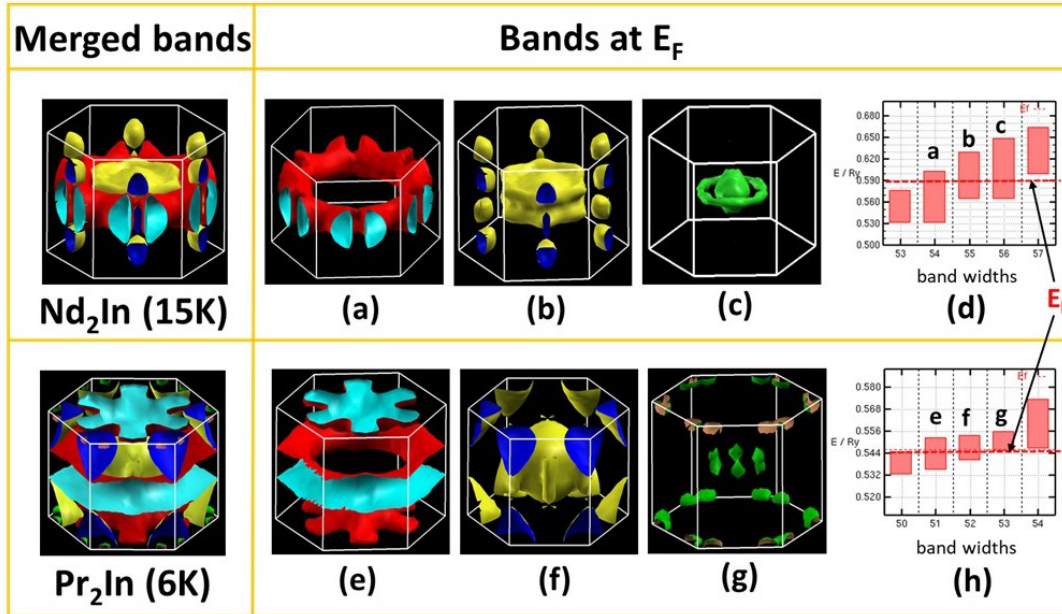
FIG. 7. (Left) Fermi surfaces in the first Brillouin zone showing majority-spin band contributions in Nd_2In and Pr_2In. (a)–(c) and (e)–(g) represent contributions of the individual bands that cross the Fermi energy (E_F) as illustrated in (d) and (h).

the left illustrate the combined Fermi surfaces of Nd_2In (top) and Pr_2In (bottom). For the first of the bands, the presence of $4f$ electrons at the Fermi energy in Pr_2In leads to electron pockets with complicated topology that appear along the $c*$ axis at the top and bottom of the Brillouin zone, in addition to a toroidal electron pocket in the middle, whereas there is a single toroidal pocket in Nd_2In in the middle [Figs. 7(e) and 7(a)]. Further, commensurate with higher total and partial DOS, presence of $4f$ states, and stronger $d-p$ hybridization at E_F [Figs. 6(b) and 6(b')] vs Figs. 6(a) and 6(a')], electron pockets in all of the three bands are larger in Pr_2In when compared to Nd_2In.

Considering that DOS of Nd_2In is different from both Pr_2In (first-order transition at T_C) and Gd_2In (second-order transition at T_C), that is, Nd $5d-$In $5p$ hybridization with a strong d character [2' in Fig. 6(a')] occurs close to but at slightly higher energy than E_F, the borderline between second- and first-order transition at T_C of Nd_2In can be ascribed to peculiar DOS features and changes in the Fermi-surface topology discussed above. Notably, lattice expansion (e.g., replacing a small fraction of Nd with La) or contraction (e.g., replacing a small fraction of In with Ga or Nd with Lu, or applying hydrostatic pressure) may shift E_F, favoring a more distinct first-order or second-order transition in doped Nd_2In. Corresponding theoretical efforts are ongoing and will be published in due time together with experimental validation of the theoretical projections.

V. SUMMARY

A large cryogenic magnetocaloric effect, observed near the boiling point of natural gas in Nd_2In, arises due to an unconventional first-order magnetic phase transition with nearly negligible thermomagnetic hysteresis. Our detailed experimental study establishes that the magnetic transition at T_C in this compound is borderline between first- and second order in nature, in contrast to the case of Pr_2In, which adopts the same Ni_2In-type hexagonal crystal structure but exhibits a more conventional first-order magnetoelastic transition. In addition to experiments, density functional theory study highlights similarities and differences in the electronic structure of these two compounds and identifies potential pathways to manipulate thermodynamic nature of the phase transition in Nd_2In with minor chemical substitutions or pressure.

[1] V. K. Pecharsky and K. A. Gschneidner, Jr., Magnetocaloric effect and magnetic refrigeration, J. Magn. Magn. Mater. **200**, 44 (1999).

[2] K. A. Gschneidner, Jr. and V. K. Pecharsky, Magnetocaloric materials, Annu. Rev. Mater. Sci. **30**, 387 (2000).

[3] V. Franco, J. S. Blázquez, J. J. Ipus, J. Y. Law, L. M. Moreno-Ramírez, and A. Conde, Magnetocaloric effect: From materials research to refrigeration devices, Prog. Mater Sci. **93**, 112 (2018).

[4] A. Kitanovski, Energy applications of magnetocaloric materials, Adv. Energy Mater. **10**, 1903741 (2020).

[5] X. Moya and N. D. Mathur, Caloric materials for cooling and heating, Science **370**, 797 (2020).

[6] W. F. Giaque and D. P. MacDougall, Attainment of temperatures below 1° absolute by demagnetization of $Gd_2(SO_4)_3$ $8H_2O$, Phys. Rev. **43**, 768 (1933).

[7] G. V. Brown, Magnetic heat pumping near room temperature, J. Appl. Phys. **47**, 3673 (1975).

[8] S. Y. Dan'kov, A. M. Tishin, V. K. Pecharsky, and K. A. Gschneidner, Jr., Magnetic phase transitions and the magnetothermal properties of gadolinium, Phys. Rev. B **57**, 3478 (1998).

[9] K. A. Gschneidner, Jr., V. K. Pecharsky, and A. O. Tsokol, Recent developments in magnetocaloric materials, Rep. Prog. Phys. **68**, 1479 (2005).

[10] Y. Mudryk, and V. K. Pecharsky, Materials for solid state cooling, in *Rare Earth Chemistry*, edited by R. Pottgen, T. Justel, and C. A. Strassert (De Gruyter, 2020), 487.

[11] F. W. Wang, X. X. Zhang, and F. X. Hu, Large magnetic entropy change in $TbAl_2$ and $(Tb_{0.4}Gd_{0.6})Al_2$, Appl. Phys. Lett. **77**, 1360 (2000).

[12] J. Cwik, T. Palewski, K. Nenkov, O. Gutfleisch, and J. Klamut, The influence of Er substitution on magnetic and magnetocaloric properties of $Dy_{1−x}Er_xCo_2$ solid solutions, Intermetallics **19**, 1656 (2011).

[13] H. Zhang, Y. J. Sun, E. Niu, L. H. Yang, J. Shen, F. X. Hu, J. R. Sun, and B. G. Shen, Large magnetocaloric effects of RFeSi (R = Tb and Dy) compounds for magnetic refrigeration in nitrogen and natural gas liquefaction, Appl. Phys. Lett. **103**, 202412 (2013).

[14] Y. Mudryk, D. Paudyal, J. Liu, and V. K. Pecharsky, Enhancing magnetic functionality with scandium: Breaking stereotypes in the design of rare earth materials, Chem. Mater. **29**, 3962 (2017).

[15] A. Biswas, T. Del Rose, Y. Mudryk, P. O. Ribeiro, B. P. Alho, V. S. R. de Sousa, E. P. Nóbrega, P. J. von Ranke, and V. K. Pecharsky, Hidden first-order phase transitions and large magnetocaloric effects in $GdNi_{1−x}Co_x$, J. Alloys Compd. **897**, 163186 (2022).

[16] P. O. Ribeiro, B. P. Alho, R. S. De Oliveira, E. P. Nobrega, V. S. R. de Sousa, P. J. von Ranke, A. Biswas, M. Khan, Y. Mudryk, and V. K. Pecharsky, Magnetothermal properties of $Ho_{1−x}Dy_xAl_2$ (x = 0, 0.05, 0.10, 0.15, 0.25 and 0.50) compounds, J. Magn. Magn. Mater. **544**, 168705 (2022).

[17] See https://igu.org/resources/global-gas-report-2020/ for Global gas report (2020). Accessed July 26, 2022.

[18] V. K. Pecharsky and K. A. Gschneidner, Jr., Giant Magnetocaloric Effect in $Gd_5(Si_2Ge_2)$, Phys. Rev. Lett. **78**, 4494 (1997).

[19] L. Morellon, P. A. Algarabel, M. R. Ibarra, J. Blasco, B. Garcia-Landa, Z. Arnold, and F. Albertini, Magnetic-field-induced structural phase transition in $Gd_5(Si_{1.8}Ge_{2.2})$, Phys. Rev. B **58**, R14721 (1998).

[20] S. B. Roy, First order magneto-structural phase transition and associated multi-functional properties in magnetic solids, J. Phys.: Condens. Matter **25**, 183201 (2013).

[21] A. Biswas, A. K. Pathak, N. A. Zarkervich, X. Liu, Y. Mudryk, V. Balema, D. D. Johnson, and V. K. Pecharsky, Designed materials with the giant magnetocaloric effect near room temperature, Acta Mater. **180**, 341 (2019).

[22] A. Biswas, N. A. Zarkevich, Y. Mudryk, A. K. Pathak, A. V. Smirnov, V. P. Balema, D. D. Johnson, and V. K. Pecharsky, Controlling magnetostructural transition and magnetocaloric effect in multi-component transition-metal-based materials, J. Appl. Phys. **129**, 193901 (2021).

[23] G. A. Govor, V. I. Mitsiuk, S. A. Nikitin, and N. Yu. Pankratov, and A. I. Smarzhevskaya, Magnetostructural phase transitions and magnetocaloric effect in Mn(As,P) compounds and their composites, J. Alloys Compd. **801**, 428 (2019).

[24] T. Krenze, E. Duman, M. Acet, E. Wassermann, X. Moya, L. Manosa, and A. Planes, Inverse magnetocaloric effect in ferromagnetic Ni-Mn-Sn alloys, Nat. Mater. **4**, 450 (2005).

[25] H. N. Bez, A. K. Pathak, A. Biswas, N. Zarkevich, V. Balema, Y. Mudryk, D. D. Johnson, and V. K. Pecharsky, Giant enhancement of the magnetocaloric response in Ni–Co–Mn–Ti by rapid solidification, Acta Mater. **173**, 225 (2019).

[26] F. Guillou, A. K. Pathak, D. Paudyal, Y. Mudryk, F. Wilhelm, A. Rogalev, and V. K. Pecharsky, Non-hysteretic first-order phase transition with large latent heat and giant low-field magnetocaloric effect, Nat. Commun. **9**, 2925 (2018).

[27] A. Fujita, S. Fujieda, Y. Hasegawa, and K. Fukamichi, Itinerant-electron metamagnetic transition and large magnetocaloric effects in $La(Fe_xSi_{1−x})_{13}$ compounds and their hydrides, Phys. Rev. B **67**, 104416 (2003).

[28] L. H. Lewis, C. H. Marrows, and S. Langridge, Coupled magnetic, structural, and electronic phase transitions in FeRh, J. Phys. D: Appl. Phys. **49**, 323002 (2016).

[29] A. Biswas, S. Gupta, D. Clifford, Y. Mudryk, R. Hadimani, R. Barua, and V. K. Pecharsky, Bulk-like first-order magnetoelastic transition in FeRh particles, J. Alloys Compd. **921**, 165993 (2022).

[30] A. Biswas, N. A. Zarkevich, A. K. Pathak, O. Dolotko, I. Z. Hlova, A. V. Smirnov, Y. Mudryk, D. D. Johnson, and V. K. Pecharsky, First-order magnetic phase transition in Pr_2In with negligible thermomagnetic hysteresis, Phys. Rev. B **101**, 224402 (2020).

[31] A. Biswas, R. K. Chouhan, O. Dolotko, A. Thayer, S. Lapidus, Y. Mudryk, and V. K. Pecharsky, Correlating crystallography, magnetism, and electronic structure across anhysteretic first-order phase transition in Pr_2In, ECS J. Solid State Sci. Technol. **11**, 043005 (2022).

[32] G. P. Zheng and J. X. Zhang, Thermal hysteresis scaling for first-order phase transitions, J. Phys.: Condens. Matter **10**, 275 (1998).

[33] M. Haldar, S. M. Yusuf, M. D. Mukadam, and K. Shashikala, Magnetocaloric effect and critical behavior near the paramagnetic to ferrimagnetic phase transition temperature in $TbCo_{2−x}Fe_x$, Phys. Rev. B **81**, 174402 (2010).

[34] Y. Mudryk, D. Paudyal, T. Prost, L. S. Chumbley, V. K. Pecharsky, and K. A. Gschneidner, Jr., Correlations between magnetism, microstructure, crystallography, and phase stability in $GdNi_{1−x}Co_x$ alloys, Acta Mater. **92**, 18 (2015).

[35] A. Biswas, Y. Mudryk, A. K. Pathak, L. Zhou, and V. K. Pecharsky, Managing hysteresis of $Gd_5Si_2Ge_2$ by magnetic field cycling, J. Appl. Phys. **126**, 243902 (2019).

[36] O. Gutfleisch, T. Gottschall, M. Fries, D. Benke, I. Radulov, K. P. Skokov, H. Wende, M. Gruner, M. Acet, P. Entel, and M. Farle, Mastering hysteresis in magnetocaloric materials, Philos. Trans. A **374**, 20150308 (2016).

[37] H. Zhang, Y. Sun, Y. Li, Y. Y. Yu, Y. Long, J. Shen, F. Hu, J. Sun, and B. G. Shen, Mechanical properties and magnetocaloric effects in $La(FeSi)_{13}$ hydrides bonded with different epoxy resins, J. Appl. Phys. **117**, 063902 (2015).

[38] F. X. Hu, B. Shen, J. Sun, and Z. Cheng, Influence of negative lattice expansion and metamagnetic transition on magnetic entropy change in the compound $LaFe_{11.4}Si_{1.6}$, Appl. Phys. Lett. **78**, 3675 (2001).

[39] I. A. Campbell, Indirect exchange for rare earths in metals, J. Phys. F: Met. Phys. **2**, L47 (1972).

[40] M. Forker, R. Müßeler, S. C. Bedi, M. Olzon-Dionysio, and S. Dionysio de Souza, Magnetic and electric hyperfine interactions in the rare-earth indium compounds R_2In studied by ^{111}Cd perturbed angular correlations, Phys. Rev. B **71**, 094404 (2005).

[41] B. P. Alho, P. O. Ribeiro, P. J. von Ranke, F. Guillou, Y. Mudryk, and V. K. Pecharsky, Free-energy analysis of the nonhysteretic first-order phase transition of Eu_2In, Phys. Rev. B **102**, 134425 (2020).

[42] D. H. Ryan, D. Paudyal, F. Guillou, Y. Mudryk, A. K. Pathak, and V. K. Pecharsky, The first-order magnetoelastic transition in Eu_2In: A ^{151}Eu Mössbauer study, AIP Adv. **9**, 125137 (2019).

[43] F. Guillou, H. Yibole, R. Hamane, V. Hardy, Y. B. Sun, J. J. Zhao, Y. Mudryk, and V. K. Pecharsky, Crystal structure and physical properties of Yb_2In and $Eu_{2-x}Yb_xIn$ alloys, Phys. Rev. Mater. **4**, 104402 (2020).

[44] W. Liu, F. Scheibel, T. Gottschall, E. Bykov, I. Dirba, K. Skokov, and O. Gutfleisch, Large magnetic entropy change in Nd_2In near the boiling temperature of natural gas, Appl. Phys. Lett. **119**, 022408 (2021).

[45] W. Cui, G. Yao, S. Sun, Q. Wang, J. Zhu, and S. Yang, Unconventional metamagnetic phase transition in R_2In (R = Nd, Pr) with lambda-like specific heat and nonhysteresis, J. Mater. Sci. Technol. **101**, 80 (2022).

[46] For details: https://www.ameslab.gov/dmse/materials-preparation-center

[47] A. P. Holm, V. K. Pecharsky, K. A. Gschneidner Jr., R. Rink, and M. N. Jirmanus, X-ray powder diffractometer for in situ structural studies in magnetic fields from 0 to 35 kOe between 2.2 and 315 K, Rev. Sci. Instrum. **75**, 1081 (2004).

[48] J. Rodriguez-Carvajal, Recent advances in magnetic structure determination by neutron powder diffraction, Physica B **192**, 55 (1993).

[49] H. Neves Bez, H. Yibole, A. Pathak, Y. Mudryk, and V. K. Pecharsky, Best practices in evaluation of the magnetocaloric effect from bulk magnetization measurements, J. Magn. Magn. Mater. **458**, 301 (2018).

[50] V. K. Pecharsky and K. A. Gschneidner Jr., Magnetocaloric effect from indirect measurements: Magnetization and heat capacity, J. Appl. Phys. **86**, 565 (1999).

[51] P. Hohenberg and W. Kohn, Inhomogeneous electron gas, Phys. Rev. **136**, B864 (1964).

[52] V. I. Anisimov, J. Zaanen, and O. K. Andersen, Band theory and Mott insulators: Hubbard U instead of Stoner I, Phys.

[53] Rev. B **44**, 943 (1991); V. I. Anisimov and O. Gunnarsson, Density-functional calculation of effective Coulomb interactions in metals, *ibid.* **43**, 7570 (1991).

[53] V. I. Anisimov, I. V. Solovyev, M. A. Korotin, M. T. Czyzyk, and G. A. Sawatzky, Density-functional theory and NiO photoemission spectra, Phys. Rev. B **48**, 16929 (1993).

[54] I. V. Solovyev, P. H. Dederichs, and V. I. Anisimov, Corrected atomic limit in the local-density approximation and the electronic structure of d impurities in Rb, Phys. Rev. B **50**, 16861 (1994).

[55] V. I. Anisimov, F. Aryasetiawan, and A. I. Lichtenstein, First-principles calculations of the electronic structure and spectra of strongly correlated systems: The LDA + U method, J. Phys.: Condens. Matter **9**, 767 (1997).

[56] P. Blaha, K. Schwarz, G. Madsen, D. Kvasnicka, and J. Luitz, WIEN2k: An augmented plane wave plus local orbitals program for calculating crystal properties, ISBN 3-9501031-1-2 (2001).

[57] P. Blaha, K. Schwarz, F.Tran, R. Laskowski, G. K. H. Madsen, and L. D. Marks, WIEN2k: An APW+lo program for calculating the properties of solids, J. Chem. Phys. **152**, 074101 (2020).

[58] J. P. Perdew, K. Burke, and M. Ernzerhof, Generalized Gradient Approximation Made Simple, Phys. Rev. Lett. **77**, 3865 (1996).

[59] I. L. M. Locht, Y. O. Kvashnin, D. C. M. Rodrigues, M. Pereiro, A. Bergman, L. Bergqvist, A. I. Lichtenstein, M. I. Katsnelson, A. Delin, A. B. Klautau, B. Johansson, I. Di Marco, and O. Eriksson, Standard model of the rare earths analyzed from the Hubbard I approximation, Phys. Rev. B **94**, 085137 (2016).

[60] T. Pandey and D. S. Parker, Magnetic properties and magnetocrystalline anisotropy of Nd_2Fe_{17}, $Nd_2Fe_{17}X_3$, and related compounds, Sci. Rep. **8**, 3601 (2018).

[61] A. Palenzona, The crystal structure and lattice constants of RE_2In and some RE_5In_3 compounds, J. Less-Common Met. **16**, 379 (1968).

[62] N. N. Delyagin, G. T. Mujiri, and V. I. Nesterov, Exchange and hyperfine interactions in the magnetic intermetallic compounds R_2In, Sov. Phys. JETP **69**, 1070 (1989).

[63] R. D. Hutchens, W. E. Wallace, and N. Nereson, Magnetic properties of Ln_3In intermetallic compounds, J. Solid State Chem. **9**, 152 (1974).

[64] H. Zhang, B. G. Shen, Z. Y. Xu, J. Chen, J. Shen, F. X. Hu, and J. R. Sun, Large reversible magnetocaloric effect in Er_2In compound, J. Alloys Compd. **509**, 2602 (2011).

[65] Q. Zhang, J. H. Cho, B. Li, W. J. Hu, and Z. D. Zhang, Magnetocaloric effect in Ho_2In over a wide temperature range, Appl. Phys. Lett. **94**, 182501 (2009).

[66] Q. Zhang, X. G. Liu, F. Yang, W. J. Feng, X. G. Zhao, D. J. Kang, and Z. D. Zhang, Large reversible magnetocaloric effect in Dy_2In, J. Phys. D: Appl. Phys. **42**, 055011 (2009).

[67] Y. S. Jia, T. Nakmiki, S. Kasai, L. W. Li, and K. Nishimura, Magnetic anisotropy and large low field rotating magnetocaloric effect in NdGa single crystal, J. Alloys Compd. **757**, 44 (2018).

[68] L. Meng, Y. Jia, Y. Qi, Q. Wang, and L. Li, Investigation of the magnetism and magnetocaloric effect in the R_2CoAl_3 (R = Gd, Tb, Dy and Ho) compounds, J. Alloys Compd. **715**, 242 (2017).

[69] J. Law, V. Franco, L. Moreno-Ramirez, A. Conde, D. Karpenkov, I. Radulov, K. P. Skokov, and O. Gutfleisch, A quantitative criterion for determining the order of magnetic phase transitions using the magnetocaloric effect, Nat. Commun. **9**, 2680 (2018).

[70] A. Biswas, T. L. Phan, N. H. Dan, A. Conde, P. Zhang, S. C. Yu, H. Srikanth, and M. H. Phan, The scaling and universality of conventional and inverse magnetocaloric effects in Heusler alloys, Appl. Phys. Lett. **103**, 162410 (2014).

[71] V. Franco, J. Y. Law, A. Conde, V. Brabander, D. Y. Karpenkov, I. Rodulov, K. Skokov, and O. Gutfleisch, Predicting the tricritical point composition of a series of LaFeSi magnetocaloric alloys via universal scaling, J. Phys. D: Appl. Phys. **50**, 414004 (2017).

[72] V. K. Pecharsky, K. A. Gschneidner, Jr., and D. Fort, Superheating and other unusual observations regarding the first order phase transition in Dy, Scr. Mater. **35**, 843 (1996).

[73] E. Mendive-Tapia, D. Paudyal, L. Petit, and J. B. Staunton, First-order ferromagnetic transitions of lanthanide local moments in divalent compounds: An itinerant electron positive feedback mechanism and Fermi surface topological change, Phys. Rev. B **101**, 174437 (2020).